Nat. Hazards Earth Syst. Sci. Discuss., 2, 2079–2102, 2014
www.nat-hazards-earth-syst-sci-discuss.net/2/2079/2014/
doi:10.5194/nhessd-2-2079-2014

Natural Hazards and Earth System Sciences
Open Access
Discussions

Sea extreme events during the last millennium in north-east of Morocco

O. Raji[1], L. Dezileau[2], U. Von Grafenstein[3], S. Niazi[1], M. Snoussi[1], and P. Martinez[4]

[1]Department of Earth Sciences, Université MohammedV-Agdal, Rabat, Morocco
[2]Geosciences, CNRS, UMR 5243 Université Montpellier 2, Montpellier, France
[3]Sciences du Climat et de l'Environnement, CNRS/CEA, Saclay, France
[4]UMR 5805 EPOC, OASU, Université Bordeaux 1, Bordeaux, France

Received: 27 January 2014 – Accepted: 23 February 2014 – Published: 15 March 2014

Correspondence to: O. Raji (otmaneraji@gmail.com) and L. Dezileau (dezileau@gm.univ-montp2.fr)

Published by Copernicus Publications on behalf of the European Geosciences Union.

Abstract

The Moroccan Mediterranean coast is located in one of the most vulnerable area to extreme weather events or tsunami hazards. The objective of this research is to reconstruct the historical extreme submersion-events record using sea-induced deposits preserved in coastal lagoon. The Nador lagoon is the largest Moroccan lagoon (115 km^2) located along the Western Mediterranean which presents a high cyclogenetic character and is exposed to tsunamis from Alboran Sea. The sandy barrier which separates the lagoon from the Mediterranean Sea is marked by many overwashes, which indicate how intensely has been exposed to the adverse sea events through history. Using the UWITEC coring platform, an undisturbed MC4.5 core (1.15 m long) was successfully sampled in the studied lagoon. To identify sea extreme events, a multi-proxy approach was applied combining sedimentogical and geochemical data. The preliminary results show that the identified paleo-events are concentrated over the last 500 years. The challenge that remains now is to distinguish between the tsunami and the storm deposits.

1 Introduction

The Mediterranean region has experienced numerous extreme coastal events, weather events (Lionello et al., 2006) as well as tsunamis events (Papadopoulos and Fokaefs, 2005) wich caused casualties and economic damages. Preventing the adverse impacts of such events requires to study their past frequency and intensity in order to predict future trends and determine their recurrence interval. However, the meteorological and marine instrumental records are limited to only a few decades especially in South Mediterranean countries. Thus, geological data offer the best way for reconstructing the historical records of intense hurricanes and tsunamis activity (Liu and Fearn, 1993). The most appropriate sites for such studies seem to be the coastal lagoons with a sandy barrier, which provide a source of material for transport and depo-

NHESSD
2, 2079–2102, 2014

sition as an overwash layer (Woodruff et al., 2008; Yu et al., 2009; and Dezileau et al., 2011).

The objective of this research is to reconstruct paleo-sea extreme events (sea storms or tsunamis) using a multi-proxy analysis in the Nador lagoon, located along the Moroccan Mediterranean coast. This area is part of the Western Mediterranean sea which presents a high cyclogenetic character (Lionello et al., 2006; Campins et al., 2006). It is also prone to risks related to tsunami events; (Gonzalez et al., 2010) have studied potential tsunamigenic sources in the Alboran sea and identified Nador area as one of the most exposed to a large tsunami wave elevation. The Nador lagoon thus offers a real potential for reconstitution of sea paleo-events, and for that an undisturbed core (MC4.5) was successfully sampled using the UWITEC coring platform in the NW of the Nador lagoon; superficial sediments were also collected during coring campaign (Fig. 1).

2 Study area

The Nador lagoon, also called Sabkha Bou Areg or Mar Chica, is the largest lagoon of Morocco with a surface area of approximately 115 km^2 and the only one located along the Moroccan Mediterranean coast between Melilla and the district of Kariat Arekman (Fig. 1). The lagoon is surrounded by a dense urbanization which houses a large population of approx. 450 000 inhabitants (RGPH, 2004). The actual development is significant and mainly related to the ongoing project of *MarchicaMed*, which covers an area of over 20 km^2 and aims to develop seven distinct cities, around the lagoon and on its barrier island. The watershed, draining an area of 220 km^2, is formed by four morphological structures: (i) in the northwest the volcanic massif of Gourougou composed of Messinien to Plio-Quaternary calc-alkaline rocks (Morel, 1985); (ii) in the west, the massif of Beni-Bou-Iffrour consists of limestones, Jurassic calcareous sandstones and marls, and of Cretaceous sandy shales and volcano-sedimentary series covered by the Miocene; (iii) in the south, the Jurassic to Mio-Pliocene Kebdana massif

NHESSD
2, 2079–2102, 2014

(Mahjoubi, 2001); and (iv) the Bou-Areg Plain in the southwest which is of Neogene to Plio-Quaternary age, characterized by salt marshes, several intermittent streams with irregular flow some of which presently serve as sewage outflows for urban areas (Irzi, 2002). Dominant climatic conditions prevailing in the study area are that of typical Mediterranean climate, with contrasted hot and dry summers, and mild and rainy winters. The strongest winds and waves are from the NE and E. Mean significant waves height is less than 1 m, although during storm condition it can reach 4.5 m (WANA Puertos del Estado wave data network). The lagoon is isolated from the Mediterranean Sea by a 25 km long sandy barrier crossed by an artificial inlet recently opened and stabilized (2011). The NW area of this lido is marked by many overwashes, which indicate how intensely it has been exposed to the adverse sea events through history.

3 Methods

The MC4.5 core was first split, photographed and logged in detail. Then, a multi-proxy approach was adopted by the combination of sedimentological, geochemical and geochronological data.

The sediment core was analyzed by X-ray fluorescence (XRF) using an XRF Core Scaner. With a step size of 0.5 mm, a semi-quantitative analysis was performed directly on the surface of sediment; this surface had to be covered with a 4 mm thin Ultralene to avoid contamination of the XRF measurement unit and desiccation of the sediment.

The analysis of particle size was performed on samples taken directly from the sediment core every cm. Using a Beckman Coulter© LS 13 320, each sample was sieved at 1 mm, suspended in deionized water and gently shaken to achieve disaggregation. After introduction of sediment into the fluid module of the granulometer, ultrasounds were used to avoid particles flocculation.

The ^{137}Cs and $^{210}Pb_{ex}$ activities analysis were measured in the fine-grained fraction (< 150 µm) by gammaspectrometry using BEGe detector (*CANBERRA BEGe 3825*). The $^{210}Pb_{ex}$ dating is based on the determination of the ^{210}Pb excess activities in the

NHESSD
2, 2079–2102, 2014

layers of the core. The use of this natural radionuclide $^{210}Pb_{ex}$ to determine sedimentation rate is now a well established technique (Goldberg, 1963; Krishnaswamy et al., 1971; Robbins and Edgington, 1975). The dating by ^{137}Cs was conducted according to Robbins and Edgington (1975). For the long scale time: the Radiocarbon (^{14}C) chronology was adopted using shell samples. ^{14}C analyses were conducted at the Laboratoire de Mesure ^{14}C ($LM^{14}C$) on the *ARTEMIS Accelerator Mass Spectrometry* in *CEA Institute at Saclay* (Atomic Energy Commission). These ^{14}C analyses were done with the standard procedure described by Tisnérat-Laborde (Tisnérat-Laborde et al., 2006).

4 Results and discussion

4.1 MC45 Core description

4.1.1 Lithostratigraphy

The MC45 sediment core of 115 cm long shows visual variations in sediment composition. Based on photography, digital X-ray radiography, stratigraphic log and grain size results (Fig. 2), the core was roughly divided into four units:

- Unit 1 (115–105 cm) composed by silty fine laminae, three colors are observed; dark grey layers and lighter grey layers correspond to fine grained sediments, while white layers associated with gypsum microcrystals correspond to relatively coarse sediments.
- Unit 2 (105–60 cm) is characterized by fine grained sediment and brownish gray color; it consists mainly of homogeneous silts with large number of shell fragments mainly at 75–100 cm interval.
- Unit 3 (60–54 cm) composed by fine parallel-laminated silts, red layers relatively fine-grained and grey layers. These laminae are well observed in digital X-ray radiography (as intercalation of dark and light laminae).

NHESSD
2, 2079–2102, 2014

– Unit 4 (54–0 cm) display several lithological changes. Three main facies can be identified: (i) silty sand characterized by coarse sediment with grey color (very dark in radiographic images) (ii) sandy silts show brownish gray color, relatively coarse sediment and is dominated by shell fragments and (iii) red silts consists in fine grained sediment with relatively absence of shell fragments.

4.1.2 Geochemistry

25 elements (Al, Si, P, S, Cl, K, Ca, Ti, V, Cr, Mn, Fe, Ni, Cu, Zn, Ga, As, Br, Rb, Sr, Y, Zr, La, Ta, Bi) were detected in the Nador MC45 core sediment; however most of them exhibit noisy profiles. Therefore, only elements which present the most important variations through depth were selected and down-core plots of signal intensity (cps, counts per second) vs. depth are presented in Fig. 3. Based on their profiles, the group composed by Al, Fe, Ti, K, Rb and Si, exhibit similar variations, intensity values are high in fine-grained intervals while low values in coarse-grained intervals. The Zr is also related to intervals rich in fine particles. However, the maximum values are only detected at the bottom of the core. The highest values of Sr and Ca are also found in the bottom but unlike to the first group, both elements show peaks in sandy layers.

4.2 Age-depth model and sedimentation rate

Measured ^{210}Pb values in the uppermost 30 cm of the MC45 core range from 132.6 to 1.7 mBq g^{-1}. In general, the downcore distribution of excess ^{210}Pb values follows a relatively exponential decrease with depth. Therefore a constant flux, constant supply CF : CS sedimentation model was applied (Appleby, 2000). The indicated sedimentation rate is about of 0.28 cm yr^{-1}.

The profile distribution of ^{137}Cs activity (Fig. 4) shows the maximum at 16 cm depth, this may represent the period of maximum radionuclide fallout in the Northern Hemisphere associated with the peak of atomic weapons testing in 1963. The ^{137}Cs-derived sedimentation rate (0.34 cm yr^{-1}) is more important than ^{210}Pb rate.

NHESSD
2, 2079–2102, 2014

Eight shells sampled from MC45 lagoon core were dated using conventional ^{14}C-AMS measurements and obtained dates were calibrated using the Marine13 curve (Reimer et al., 2013) (Table 1). The modern ^{14}C reservoir age in Nador lagoon was estimated using the radiocarbon date within $^{210}Pb_{ex}$-time domain. Sea surface reservoir ^{14}C ages $R(t)$ for the modern shell (SacA 28609) were calculated by subtracting the atmospheric ^{14}C value estimated for the historical date AD 1930 (152 ± 7 ^{14}C yr, Reimer et al., 2013) from the measured apparent ^{14}C ages of the mollusk (235 ± 30 ^{14}C yr, Table 3, Fig. 3). This gives a $R(t)$ value of 83 yr. The deviance from the global mean reservoir age (ΔR) is then obtained by subtracting the marine model age value estimated for AD 1930 (453 ± 23 ^{14}C yr, (Reimer et al., 2013)) from the measured apparent ^{14}C age of the shell (235 ± 30 ^{14}C yr, Table 3, Fig. 3). The ΔR of about -218 years is thus estimated and adopted (Table 2). The negative ΔR value is common in shallow oceanic regions or in enclosed lagoons where (i) the ^{14}C in seawater DIC (dissolved inorganic carbon) are higher than the average global ocean, and (ii) ^{14}C mixing with depleted water from deeper ocean is limited (Dutta, 2008). However, this value should be taken with caution, due to: (i) intra-shell variation in radiocarbon age, which can be significant (~ 200 y) (Jones et al., 2007) and (ii) to possible variations in relation to palaeo-environmental changes (Sabatier et al., 2010).

The age model of MC45 core was realized by fitting a linear regression using the "clam" R-code package version 2.2 (Blaauw, 2010) on ^{14}C ages (without inversed ages) and $^{210}Pb_{ex}/^{137}Cs$ (Fig. 5). The ^{14}C mean sedimentation rate calculated is $0.10\,cm\,yr^{-1}$.

4.2.1 Sediments source

The sedimentation in Nador lagoon is mostly controlled by terrestrial and marine inputs. Rivers are the main source of fine sediments dispersed within the lagoon while marine sediments consist mainly of coarse carbonate sand (Inani, 1995; Mahjoubi, 2001 and Bloundi, 2005). In order to characterize the lagoon barrier beach sand samples, the

NHESSD
2, 2079–2102, 2014

spectrum of the grain size percentages vs. grain size was plotted; the results show unimodal distribution with one mean grain population ranging between 133 and 282 µm. The percentages of this grain size class in surface samples decrease considerably from the sea to the lagoon (Fig. 6), therefore, it can be used successfully to trace marine sand in lagoon sediments.

The geochemical data obtained by XRF portable analyzer allowed detection of 11 elements (Ti, Fe, Sr, Cu, Zn, Zr, Mn, Co, As, Rb, and Pb). Variation of the concentration of the most important detected elements from sea to continental samples (Fig. 7) shows that the elemental composition of barrier beach sediments are enriched in Sr and depleted in Fe, Ti, Mn and Rb. Although, these results are based on a limited number of samples and detected elements, they are in agreement with previous studies in the area. Indeed, in Nador lagoon two groups can be identified: the first group is composed of Al, Fe, K, Mn, S, Ti and Mg, these elements are associated with clay and Feldspar and the minimum concentrations are found mainly on the continental part of the lagoon. The second group is composed of Ca and Sr the calcium being mainly of marine origin, associated to biogenic calcareous (Bloundi, 2005). Regarding Si, its terrestrial origin is mainly from feldspar and clay minerals while the marine Si comes from mainly from quartz.

In order to trace marine sediment geochemically, inter-elements ratios of terrestrial elements and marine elements can be used. Additionally, the use of inter-elements ratios presents the advantage to be insensitive to dilution and matrix effects (Richter et al., 2006; Croudace et al., 2006).

4.2.2 Identification of paleoevents

The evolution with depth of the 133–282 µm grain size population in MC45 core shows five peaks; all are over the last 600 years. However, only three events are confirmed by geochemical data (Fig. 8). Indeed, the selected inter-elements ratios (Si/Al, Ca/Fe and Sr/Fe) show important peaks for the events 1, 2 and 3. An increase of inter-elements ratios value is also observed in the bottom core, this is not related to the presence of

NHESSD
2, 2079–2102, 2014

coarse sediments but to the gypsum crystals (enriched en Ca and Sr and depleted en Al and Fe).

Based on all of the above results, we can confidently assume that the events 1, 2 and 3 correspond to paleo-overwash events. The age model indicates that overwash layer "1" was probably deposited between Cal AD 1438 to 1524, the overwash "2" between Cal AD 1610 to 1799 and overwash "3" between Cal AD 1856 to 1899.

4.3 Storm or tsunami events?

Generally, both tsunamis and storms cause brief coastal flooding with high overland flow velocities. Distinguishing tsunami and storm deposits is still controversial and several studies have pointed out many hypotheses regarding the diagnostic characteristics of storm/tsunami deposits (Kortekaas and Dawson, 2007; Morton et al., 2007; Tappin, 2007; Engel and Brückner, 2011).

Local and regional historic documents with tsunami catalogues are one of the best ways to correlate identified events with historical recorded tsunamis or storm events. During the last 600 years four tsunamis were recorded in the western Mediterranean coast; (i) the 22 September 1522 tsunami near Almeria coast (Spain); recently evidences of this tsunami deposits were found in Cabo de Gata lagoon (Reicherter and Heidmann, 2009). In Moroccan Mediterranean coast, the affected areas are mainly Badis Ghomera (Al Hoceima); however, this information is not supported by Maghrebian documents (Kaabouben et al., 2009). Anyway, the geographic position of Nador lagoon directly exposed lets us not exclude its impact on Nador area. (ii) The 9 October 1680 tsunami (Malaga) is not supported by the available information in contemporary documents (Goded et al., 2008). Besides, Nador lagoon is not geographically exposed. (iii) The 9 October 1790 tsunami which caused flooding of the north shore of Africa and southern shore of Spain (Soloviev, 2000). No documents support tsunami waves on the Moroccan coast but the extent of the tsunami event on Algeria coast and its manifestation on the southern coast of Spain, leads to assume a possible impact on the northern Moroccan coast (Kaabouben et al., 2009). (iv) Finally, the 21

NHESSD
2, 2079–2102, 2014

August 1856 of this tsunami on the north-eastern shore of Algeria (Jijel, 300 km east of Algiers) (Salaviev, 2000); the effects of this event on the Moroccan coasts is improbable (Kaabouben et al., 2009).

In the Nador area, the well recorded sea storms are those who opened inlets along the lagoon lido. The oldest one is the 1889 strong storm caused by N to NE winds and which occasioned a large inlet of 150 m width. The paleo-inlets 3 and 5 (Fig. 1) were respectively the results of recent storms of 1941 and 1981. The inlet 1 was opened artificially in 1909 but enlarged by storms effects. In addition, it should be noted that in the Western Mediterranean, storms had a higher frequency in the Little Ice Age (LIA), with two lesser periods of high frequency in the 1400s and at the end of the 1700s (Camuffo et al., 2000). Other studies confirmed increased intensity and frequency of storms during the LIA in the Mediterranean, as for example in the French coast (Dezileau et al., 2011). Based on a set of six simulations of the LIA using an Ocean–Atmosphere General Circulation Model (OAGCM), Raible et al. (2006) consistently found an increase in cyclone occurrence in the Mediterranean during the LIA compared to present-day.

Considering all these historical data, we can confidently assume that the event 3 corresponds to 1889 storms because of its date located in "the event 3" age interval and also of the paleo-overwash generated by this event located in front of the coring site. For the event 1 and 2, the tsunami-storm hypothesis remains open. Indeed, even if they are probably related to sea storms because of the increase of these phenomena during this period in the Western Mediterranean, both 1522 and 1790 tsunamis seem to have also affected the Nador area during event interval age 1 and 2 respectively. Based on examples of modern tsunami and storm deposits, some sedimentological criteria can be used to identify tsunami from storm deposit (Morton et al., 2007). The tsunami deposit has a relatively thin bed consisting of a single structureless bed or a bed with only a few thin layers. The presence of internal mud laminae or intraclasts is more in favor of tsunami deposits. The storm origin deposit present a moderately thick sand bed composed of numerous subhorizontal planar laminations organized into multiple laminasets. The stratification associated with bed-load transport and abundant shell frag-

NHESSD
2, 2079–2102, 2014

ments organized in laminations also favor a storm origin. In our case, all of the events deposits identified are observed as a single homogeneous bed (~ 2–5 cm thick). Within it, no sedimentary structures (ripple crossbeds, planar laminae or mud intraclasts) were observed; only the events 3 contain internal mud laminae within the deposit. However, even if these criteria favor tsunami origin, this observation should be taken with caution because the use of a single sediment core results make it inadequate for physical distinction process (Morton et al., 2007). About the use of geochemical signatures to distinguish between tsunami and storm deposits, no study was found. The increase in geochemical elements indicating marine origin as evidence of marine inundation is generally used in both deposits (Engel et al., 2010; Ramírez-Herrera et al., 2012).

5 Conclusions

The present study is a first attempt for the reconstitution of paleo-events in the Nador lagoon; he use of a multiproxy analysis by lithological evidences and X-ray fluorescence has revealed distinct anomalies and allowed differentiation of stratigraphic intervals which are interpreted as event horizons. Eight radiocarbon dates of shells samples combined with ^{210}Pb and ^{137}Cs chronologies allowed to establish a chronological framework, which was used to calculate a time-averaged sedimentation rate (0.10 to 0.28 cm year^{-1}).

Three events were identified; all of them are concentrated over the last 500 years. Attribute these deposits to tsunami or storm events was not an easy task; historically only the modern event can be attributed with certainty to a 1889 major storm. The sedimentological and geochemical data were not very helpful in this process because of the single core studied but they could probably be more indicative by correlation with other cores in the area.

Acknowledgements. The authors would like to all participants in the coring expedition, particularly O. Ther (Technician, U. Bordeaux), E. Regnier (Technician, LSCE – IPSL, Paris) and P. Blanchemanche (Pr. Archeo-Montpellier) for their collaboration in the various stages of this

NHESSD
2, 2079–2102, 2014

study. The authors wish to thank also the staff of *MarChica Med* Company (Rabat and Nador) for their assistance during the entire period of the expedition. This study is funded by the MISTRAL project (Coord. L. Dezileau) and PHC-Volubilis (MA/11/253; coord.: L. Dezileau and M. Snoussi).

References

Blaauw, M.: Methods and code for "classical" age-modelling of radiocarbon sequences, Quat. Geochronol., 5, 512–518, 2010.

Bloundi, M. K.: Etude géochimique de la lagune de Nador (Maroc oriental): impacts des facteurs anthropiques, Ph.D. thesis, Univ. Louis Pasteur, France & Univ. Mohammed V-Agdal, Maroc., 238 p., 2005.

Campins, J., Jansà, A., and Genovés, A.: Three-dimensional structure of western Mediterranean cyclones, Int. J. Climatol., 26, 323–343, 2006.

Camuffo, D., Secco, C., Brimblecombe, P., and Martin-Vide, J.: Sea storms in the Adriatic Sea and the Western Mediterranean during the last millennium, Climatic Change, 46, 209–223, 2000.

Dezileau, L., Sabatier, P., Blanchemanche, P., Joly, B., Swingedouw, D., Cassou, C., Castaings, J., Martinez, P., and Von Grafenstein, U.: Intense storm activity during the Little Ice Age on the French Mediterranean coast, Palaeogeogr. Palaeocl., 299, 289–297, 2011.

Dutta, K.: Marine ^{14}C reservoir age and Suess Effect in the Indian Ocean, Earth Science India, 1, 243–257, 2008.

Engel, M., Brückner, H., Wennrich, V., Scheffers, A., Kelletat, D., Vött, A., Schäbitz, F., Daut, G., Willershäuser, T., and May, S. M.: Coastal stratigraphies of eastern Bonaire (Netherlands Antilles): new insights into the palaeo-tsunami history of the southern Caribbean, Sediment. Geol., 231, 14–30, 2010.

Engel, M. and Brückner, H.: The identification of palaeo-tsunami deposits – a major challenge in coastal sedimentary research, Dynamische Küsten – Grundlagen, Zusammenhänge und Auswirkungen im Spiegel angewandter Küstenforschung, in: Proceedings of the 28th Annual Meeting of the German Working Group on Geography of Oceans and Coasts, 22–25, 2011.

Goldberg, E.: Geochronology with lead-210, International Atomic Energy Agency, 121–131, 1963.

NHESSD

2, 2079–2102, 2014

Gonzalez, M., Medina, R., Olabarrieta, M., and Otero, L.: Tsunami hazard assessment on the southern coast of Spain, Turk. J. Earth Sci., 19, 351–366, 2010.
Inani, I.: Dynamique sédimentaire et état de la pollution dans la lagune de Nador, Ph.D. thesis, Univ. Mohamed V, Fac. Sci. Rabat, 186 pp., 1995.
Irzi, Z.: Les Environnements du Littoral méditerranéen du Maroc compris entre l'oued Kiss et le Cap des trois Fourches dynamique sédimentaire et évolution et écologie des foraminifères benthiques de la lagune de Nador, Ph.D. thesis, Univ. Mohammed I, Oujda, 279 pp., 2002.
Jones, K. B., Hodgins, G. L., Dettman, D. L., Andrus, C., Nelson, A., and Etayo-Cadavid, M. F.: Seasonal variations in Peruvian marine reservoir age from pre-bomb *Argopecten purpuratus* shell carbonate, Radiocarbon, 49, 877–888, 2007.
Kaabouben, F., Baptista, M. A., Iben Brahim, A., El Mouraouah, A., and Toto, A.: On the moroccan tsunami catalogue, Nat. Hazards Earth Syst. Sci., 9, 1227–1236, doi:10.5194/nhess-9-1227-2009, 2009.
Kortekaas, S. and Dawson, A.: Distinguishing tsunami and storm deposits: an example from Martinhal, SW Portugal, Sediment. Geol., 200, 208–221, 2007.
Krishnaswamy, S., Lal, D., Martin, J., and Meybeck, M.: Geochronology of lake sediments, Earth Planet. Sc. Lett., 11, 407–414, 1971.
Lionello, P., Bhend, J., Buzzi, A., Della-Marta, P., Krichak, S., Jansa, A., Maheras, P., Sanna, A., Trigo, I., and Trigo, R.: Cyclones in the Mediterranean region: climatology and effects on the environment, Dev. Earth Env. Sci., 4, 325–372, 2006.
Liu, K.-B. and Fearn, M. L.: Lake-sediment record of late Holocene hurricane activities from coastal Alabama, Geology, 21, 793–796, 1993.
Liu, K. B., Shen, C., and Louie, K. S.: A 1,000-year history of typhoon landfalls in Guangdong, Southern China, reconstructed from Chinese historical documentary records, Ann. Assoc. Am. Geogr., 91, 453–464, 2001.
Mahjoubi, R.: Nature et origine du flux de matières particulaires et son enregistrement dans un milieu paralique microtidal: cas de la lagune de Nador (Maroc nord oriental), Ph.D. thesis, Univ Moulay Ismail, Meknès, 273 pp., 2001.
Morel, J. L.: Les événements tectoniques et volcaniques responsables de la regression messinienne dans le Maroc septentrional: exemple du bassin d'Iaddouyine (Segangane-Rif Oriental-Maroc), Bulletin de l'Institut Scientifique, Rabat, 97–106, 1985.
Morton, R. A., Gelfenbaum, G., and Jaffe, B. E.: Physical criteria for distinguishing sandy tsunami and storm deposits using modern examples, Sediment. Geol., 200, 184–207, 2007.

NHESSD
2, 2079–2102, 2014

Papadopoulos, G. A. and Fokaefs, A.: Strong tsunamis in the Mediterranean Sea: a re-evaluation, ISET J. Earthquake Technol., 42, 159–170, 2005.
Ramírez-Herrera, M.-T., Lagos, M., Hutchinson, I., Kostoglodov, V., Machain, M. L., Caballero, M., Goguitchaichvili, A., Aguilar, B., Chagué-Goff, C., and Goff, J.: Extreme wave deposits on the Pacific coast of Mexico: tsunamis or storms? – a multi-proxy approach, Geomorphology, 139, 360–371, 2012.
Reimer, P. J., Bard, E., Bayliss, A., Beck, J. W., Blackwell, P. G., Ramsey, C. B., Grootes, P. M., Guilderson, T. P., Haflidason, H., and Hajdas, I.: IntCal13 and Marine13 radiocarbon age calibration curves 0–50,000 years cal BP, Radiocarbon, 55, 1869–1887, 2013.
Robbins, J. A. and Edgington, D. N.: Determination of recent sedimentation rates in Lake Michigan using Pb-210 and Cs-137, Geochim. Cosmochim. Ac., 39, 285–304, 1975.
Sabatier, P., Dezileau, L., Blanchemanche, P., Siani, G., Condomines, M., and Bentaleb, I.: Holocene variations of radiocarbon reservoir ages in a Mediterranean lagoonal system, Radiocarbon, 52, 91–102, 2010.
Tappin, D. R.: Sedimentary features of tsunami deposits – their origin, recognition and discrimination: an introduction, Sediment. Geol., 200, 151–154, 2007.
Tisnérat-Laborde, N., Poupeau, J., Tannau, J., and Paterne, M.: Development of a semi-automated system for routine preparation of carbonate samples, Radiocarbon, 43, 299–304, 2006.
Woodruff, J. D., Donnelly, J. P., Mohrig, D., and Geyer, W. R.: Reconstructing relative flooding intensities responsible for hurricane-induced deposits from Laguna Playa Grande, Vieques, Puerto Rico, Geology, 36, 391–394, 2008.
Yu, K.-F., Zhao, J.-X., Shi, Q., and Meng, Q.-S.: Reconstruction of storm/tsunami records over the last 4000 years using transported coral blocks and lagoon sediments in the southern South China Sea, Quatern. Int., 195, 128–137, 2009.

NHESSD
2, 2079–2102, 2014

Table 1. ^{14}C data for mollusk shells from MC45. ^{14}C ages are calibrated using the Marine13 calibration curve with reservoir age ΔR of −218, model. Ages were obtained by Clam code-package.

Lab code	Depth (cm)	$\delta^{13}C$ ‰	^{14}C ages (BP)	Clam Model ages (AD)
SacA 28609	22	4.8	235 ± 30	1854 ± 93
SacA 26943	32	2.40	730 ± 30	1393 ± 62*
SacA 26944	46	0.70	575 ± 30	1537 ± 76
SacA 26945	50	2.4	630 ± 30	1476 ± 48
SacA 28610	56	3.8	645 ± 30	1464 ± 45*
SacA 28611	64	4	620 ± 30	1483 ± 47
SacA 26946	91	4.40	1340 ± 30	831 ± 91*
SacA 26947	104	6.50	1035 ± 30	1149 ± 87

(*) inversed ages

NHESSD
2, 2079–2102, 2014

Table 2. ^{14}C date of modern pre-bomb shell samples in MC45 core and its reservoir ages. Estimation of $R(t)$ and ΔR were estimated using the $^{210}Pb_{ex}$ date.

Lab code	^{210}Pb age (AD)	^{14}C yr (BP)	Tree-ring ^{14}C age (BP) IntCal13	Reservoir age $R(t)$ (yr)	Model age (Marine13 curve)	ΔR (yr)
SacA 28609	1930	235 ± 30	152 ± 7	83	453 ± 23	−218

NHESSD
2, 2079–2102, 2014

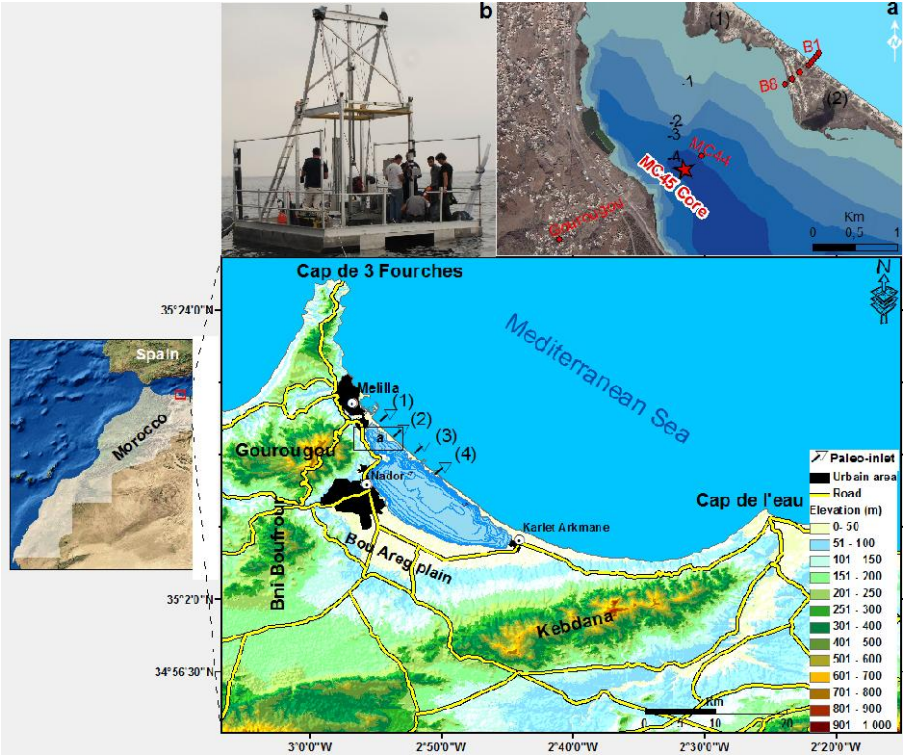

Fig. 1. Map of the study area (Nador lagoon): **(a)** the location of surface samples and the MC45 core sampled in NW of Nador Lagoon. **(b)** UWITEC coring platform used in Nador campaign.

NHESSD
2, 2079–2102, 2014

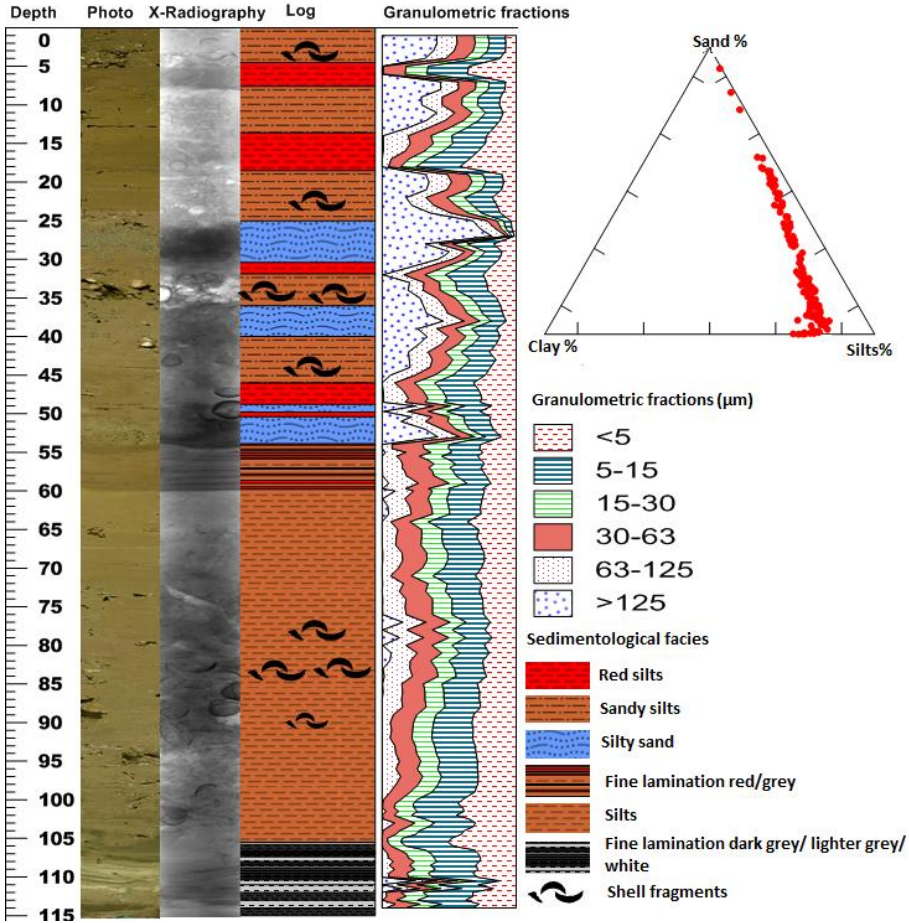

Fig. 2. Photography, digital X-ray radiography, stratigraphic log and grain size results of MC45 core.

NHESSD
2, 2079–2102, 2014

Sea extreme events during the last millennium

O. Raji et al.

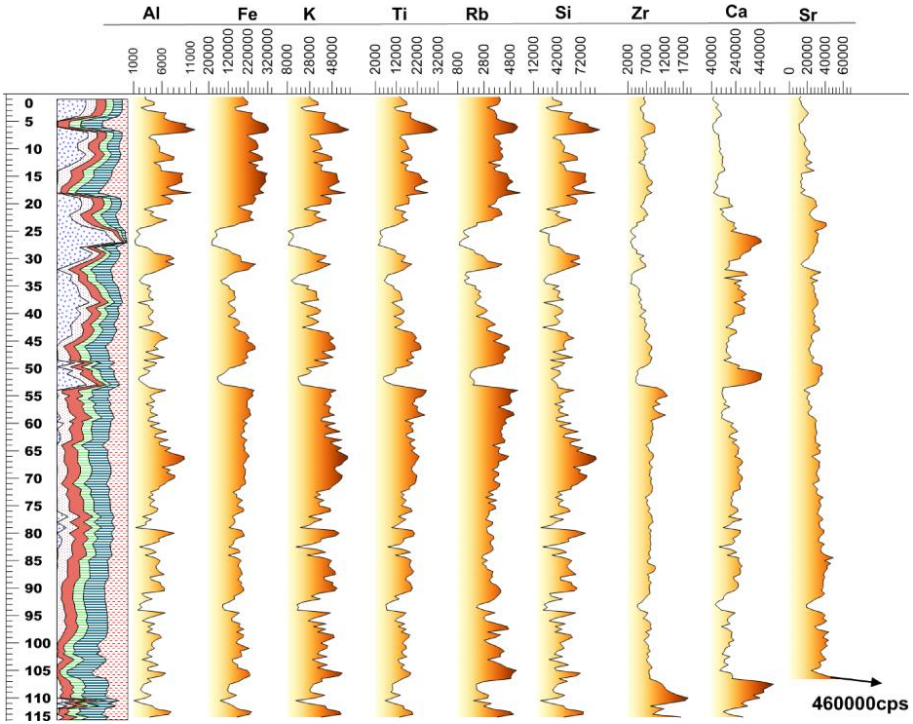

Fig. 3. Down-core plots of signal intensity (cps, counts s^{-1}) vs. depth in MC45 of nine geochemical elements.

NHESSD
2, 2079–2102, 2014

Sea extreme events during the last millennium

O. Raji et al.

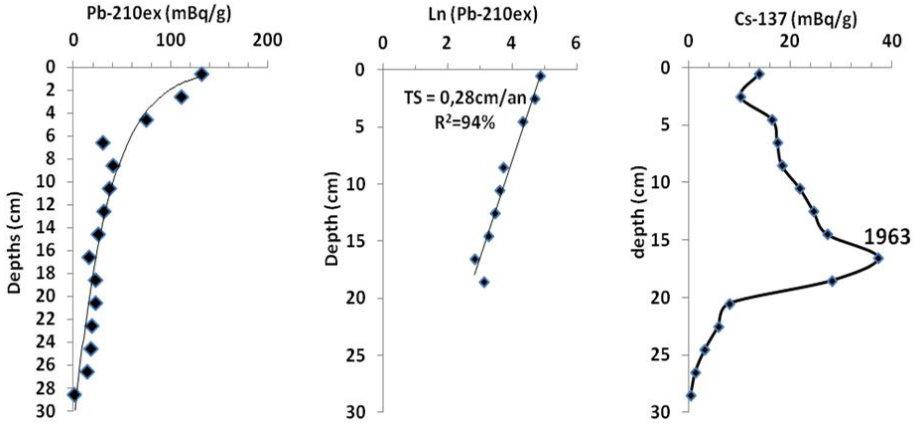

Fig. 4. Profile distributions of $^{210}Pb_{ex}$ and ^{137}Cs activity concentration vs. depth in MC45 core. Using the CFCS model, the ^{210}Pb data indicate a sedimentation rate of 0.28 cm yr^{-1}. The activity depth profile ^{137}Cs displays a peak at 16 cm, resulting in accumulation rates of 0.3 cm yr^{-1} for the 1963 depths.

NHESSD
2, 2079–2102, 2014

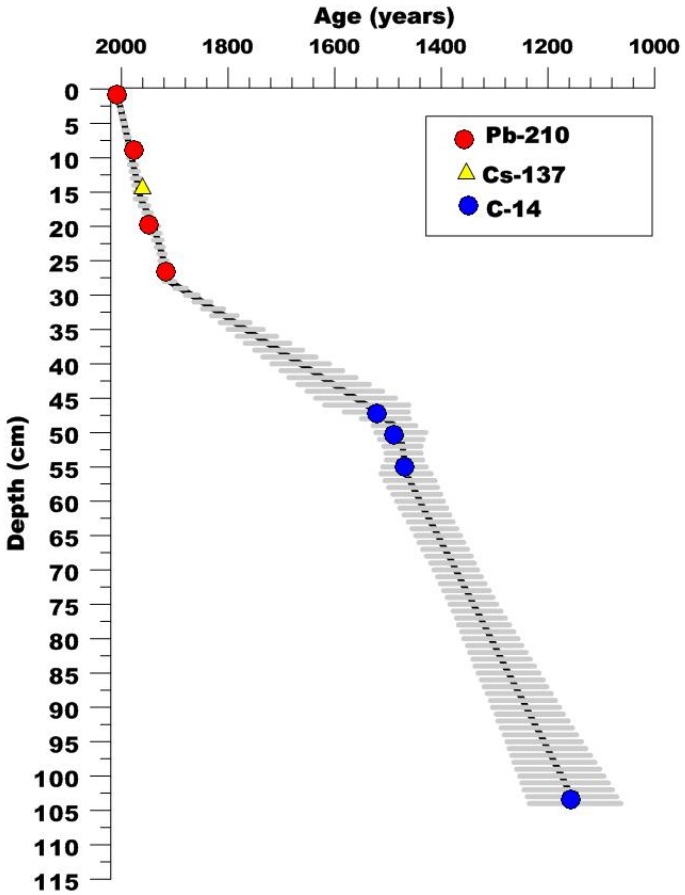

Fig. 5. Stratigraphic age–depth plot undertaken in CLAM (Blaauw, 2010) of MC45 core. CLAM settings: linear interpolation; 1000 iterations weighted by calibrated probabilities at 95 % confidence ranges and resolution 1 year steps. CLAM output statistics: 0–104 cm with age reversals were removed.

NHESSD
2, 2079–2102, 2014

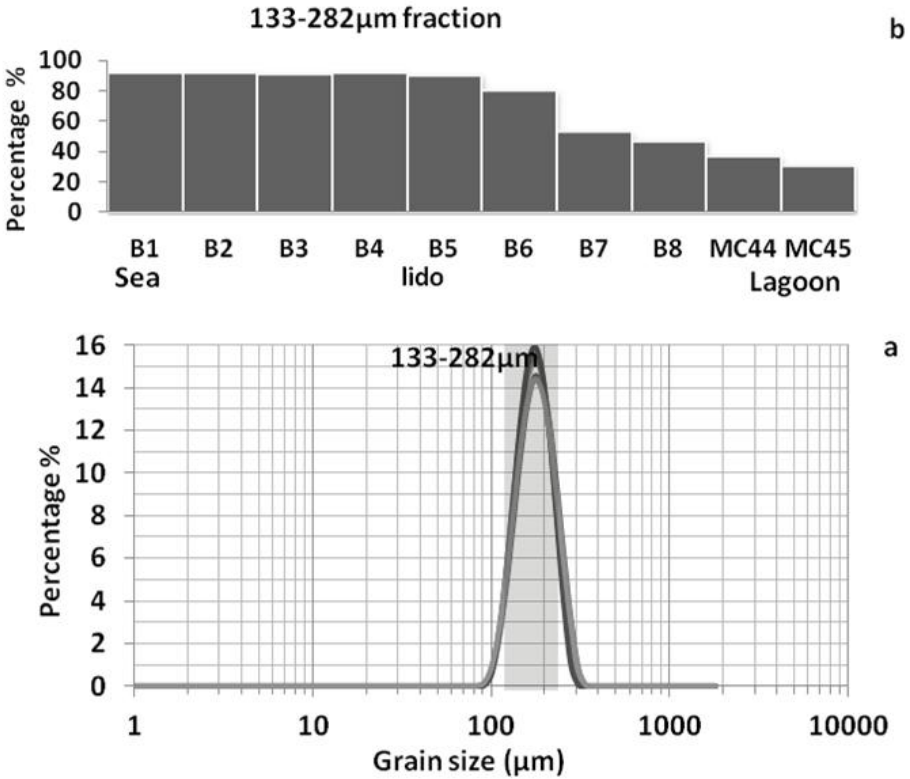

Fig. 6. Grain size of lido sand in Nador lagoon. **(a)** The spectrum of the grain size percentages vs. grain size with unimodal distribution (133 and 282 µm). **(b)** Distribution of 133–282 fraction along sea–lagoon transect.

NHESSD
2, 2079–2102, 2014

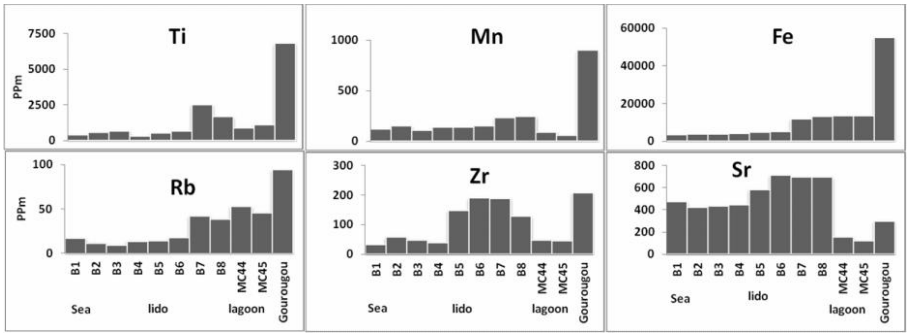

Fig. 7. Distribution of geochemical elements concentration (ppm) along sea–lagoon–continental board transect.

NHESSD
2, 2079–2102, 2014

Sea extreme events during the last millennium

O. Raji et al.

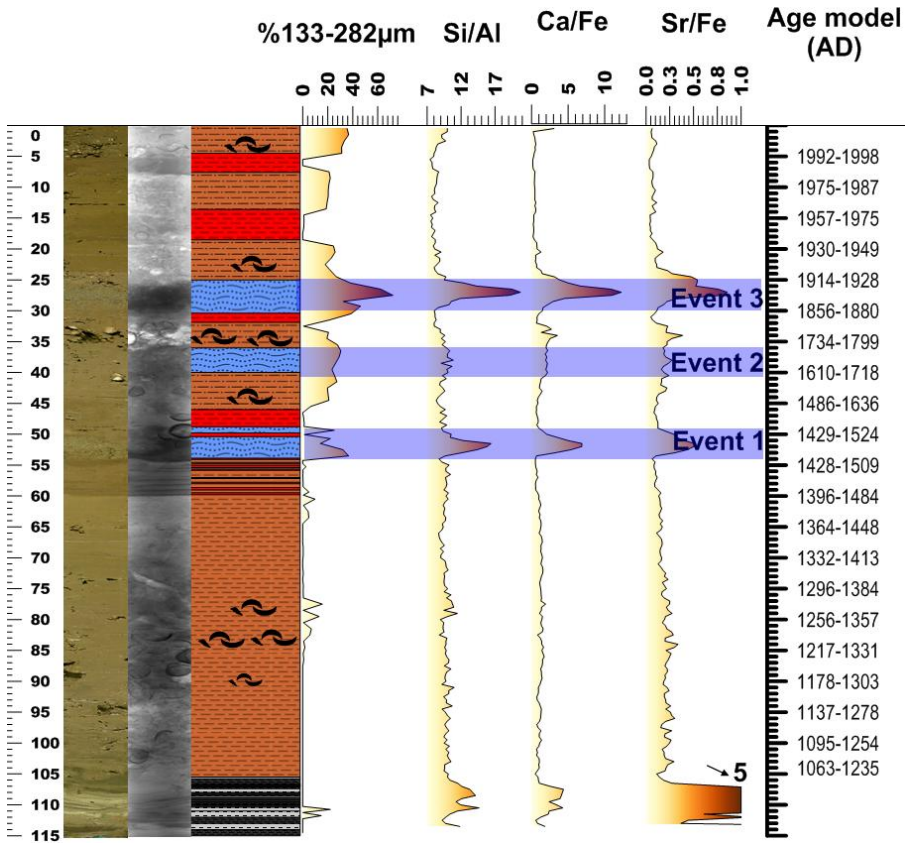

Fig. 8. Identification of paleo-events based on photography, radiography X, log, grain size and geochemical inter-elements ratios. The identified events show coarse grained texture in photography, dark layer in radiography X, high percentage of 133–282 µm fraction and peaks of Si/Al, Ca/Fe and Sr/Fe ratios.

NHESSD
2, 2079–2102, 2014